Convection-driven melting in an n-octane pool fire bounded by an ice wall

Farahani, Hamed Farmahini ; Alva, Wilson Ulises Rojas; Rangwala, Ali S.; Jomaas, Grunde

Published in:
Combustion and Flame

Link to article, DOI:
10.1016/j.combustflame.2017.02.006

Publication date:
2017

Document Version
Peer reviewed version

Convection-driven melting in an n-octane pool fire bounded by an ice wall

Hamed Farmahini Farahani[a*], Wilson Ulises Rojas Alva[b], Ali S. Rangwala[a], Grunde Jomaas[b]

[a] Department of Fire Protection Engineering, Worcester Polytechnic Institute, Worcester, MA 01609, USA

[b] Technical University of Denmark (DTU), Department of Civil Engineering Brovej, Building 118 DK-2800 Kgs. Lyngby, Denmark

***Corresponding Author:**

Hamed Farmahini Farahani

100 Institute Road, Worcester, MA 01609 USA

Phone: 1-508-831-5027

Fax: 1-508-831-5862

E-mail: ffarahani.hamed@gmail.com

Type of Article:

Full Length Article

Abstract

An experimental study on an n-octane pool fire bound on one side by an ice wall was carried out to investigate the effects on ice melting by convection within the liquid part of the fuel. Experiments were conducted in a square glass tray (9.6 cm × 9.6 cm × 5 cm) with a 3 cm thick ice wall (9.6 cm × 6.5 cm × 3 cm) placed on one side of the tray. The melting front velocity, as an indicator of the melting rate of the ice, increased from 0.04 cm/min to 1 cm/min. The measurement of the burning rates and flame heights showed two distinctive behaviors; an induction period from the initial self-sustained flame to the peak mass loss rate followed by a steady phase from the peak of mass loss rate until the manual extinguishment. Similarly, the flow field measurements by a 2-dimensional PIV system indicated the existence of two different flow regimes. In the moments before ignition of the fuel, coupling of surface tension and buoyancy forces led to a combined one roll structure in the fuel. After ignition the flow field began transitioning toward an unstable flow regime (separated) with an increase in number of vortices around the ice wall. The separated regime started with presence of a multi-roll structure

separating from a primary horizontal flow on the top driven by Marangoni convection. As the burning rate/flame height increased the velocity and evolving flow patterns enhanced the melting rate of the ice wall. Experimentally determined temperature contours, using an array of finely spaced thermocouples in the liquid fuel, were used to further investigate the two layer temperature structure; an upper layer (~8 mm thick) with steep temperature gradient in the vertical direction and a layer of low temperature in deeper regions. A hot zone with thickness of ~3 mm was present below the free surface corresponding to the multi-roll location. The multi-roll structure could be the main reason for the transport of the heat received from the flame toward the ice wall which causes the melting.

Keywords: convective flow, melting, n-octane, pool fire, ice wall.

1. Introduction

The behavior and characteristics of pool fires have been studied for decades, including convective motions in the liquid. Understanding the controlling mechanisms of the liquid-phase convection in pool fires have aided fire researchers in explaining ignition and flame spread problems [1, 2]. When the temperature of the liquid pool is lower than the liquid flash point temperature, liquid-phase convection becomes a key point for both ignition and flame spread process [3, 4]. Due to the convection in the liquid phase, the heat required for creating a vapor concentration equal to the lean-limit concentration for a gaseous fuel-air mixture is removed, causing a delay in ignition [5-7]. Conversely, flame spread is powered by the convective flows in the liquid-phase [8]. This flow is mainly governed by surface tension and viscous forces and slightly by gravity [9, 10]. A fairly recent scaling study on flame spread [11] presented flow structures and pulsating regimes indicating the magnitude of convection on the bulk and surface of the liquid fuels.

There is an extensive collection of both theoretical and experimental articles on the subject of flame spread, as reviewed by Glassman and Dryer [12]. However, few studies have addressed the transport phenomena in the liquid-phase throughout the burning time of the pool fires [13-15]. Furthermore, the effects of convective flow on the walls of the pool were dismissed until a new practical problem emerged; burning of oil spills in ice-infested regions e.g. burning of spilled oil in ice cavities or melt-pools. It is shown that removing the spilled oil in ice-infested regions is promising via in-situ burning [16-18]. This also opens up a new area of research

related to understanding the influence of ice melting on pool fire burning dynamics, which is the focus of the current study.

In typical pool fires, bounded with rigid sidewalls, a portion of the heat produced by the flame transfers to the body of the fuel in deeper areas through the walls and creates upward convective flows in the liquid adjacent to the wall [19]. When the pool is bounded by walls of ice, the transport mechanisms are significantly altered [20]. Previous studies on burning of liquid fuels in ice cavities exhibited a convection-melt phenomenon which is referred as "*lateral cavity formation*". During burning of liquid fuels inside ice cavities [20-22] the burning fuel was observed to melt the ice and create an ice lip. The ice melting process was found to be more significant in the regions of the fuel layer contact with the ice versus regions of flame impingement. The observations made during experiments of a previous study [23] supported existence of a flow close to the free surface of the fuel. It was hypothesized that the formation of lateral cavities is due to the convective flows in the liquid fuel layer driven by buoyancy and surface tension, relating to natural and Marangoni convection, respectively.

The objective of this study is to visualize the flow in the fuel layer using Particle Image Velocimetry (PIV) technique and to analyze the flow characteristics coupled with the temperature field. Exploring the extent of convective flows could explain the causes for melting of the ice and formation of the lateral cavity. Most oil spills happen in large size (pool size of several meters or larger) and involve multi-component fuels. The insight provided by laboratory-scale experiments on pure liquid fuels along with large scale pool fires in ice are useful to understand the controlling thermo-physical parameters and effect of the geometry [24]. It is envisioned that the results of this study can add to the current knowledge on the convection-driven melting process of ice.

2. Experimental Setup

The experimental setup was developed to observe the melting of the ice and investigate convective flows within the liquid phase of an n-octane pool fire. A schematic of the experimental setup is shown in Fig. 1. The custom-made borosilicate glass tray used for the burning (2 mm wall thickness) was an open top square with outside dimensions of 100 × 100 mm and a depth of 50 mm. The liquid fuel used herein was n-octane, which has a Prandtl number well above unity (7.8), density of 703 kg/m^3 and a boiling point of 125 °C as the liquid fuel. Each experiment used a 96 × 60 × 30 mm ice wall placed on one side of the tray as shown

with dark color in Fig. 1 (a) and (b). In order to create ice wall free of visual imperfections, demineralized water was frozen using a directional freezing method, thus preventing the inclusions of gas bubbles and other impurities. A bracket-shaped holder (shown with dashed line in Fig. 1) was used to keep the ice wall fixed at the wall of the tray. A base-layer of water with initial temperature of 0-2 °C was poured into the tray to a depth of 20 mm, followed by an n-octane layer that was 15 mm thick and had a temperature of 10-12 °C. The tray was then placed on a load cell (0.01 g precision) to record mass loss. A camera was placed in front of the test setup to capture the flame heights during the burning process. A propane torch igniter was used to ignite the fuel layer after it was poured into the tray.

Preliminary tests with and without the ice wall were repeated three times to ensure the reproducibility of the results. The burning duration, mass loss, and flame height were experimentally determined. The flame height was measured by capturing random frames each four seconds from the videos of the tests. Then, the flame height was measured for each image via ImageJ [25]. The measured flame heights of each test were averaged to obtain an average flame height for the duration of the n-octane burning.

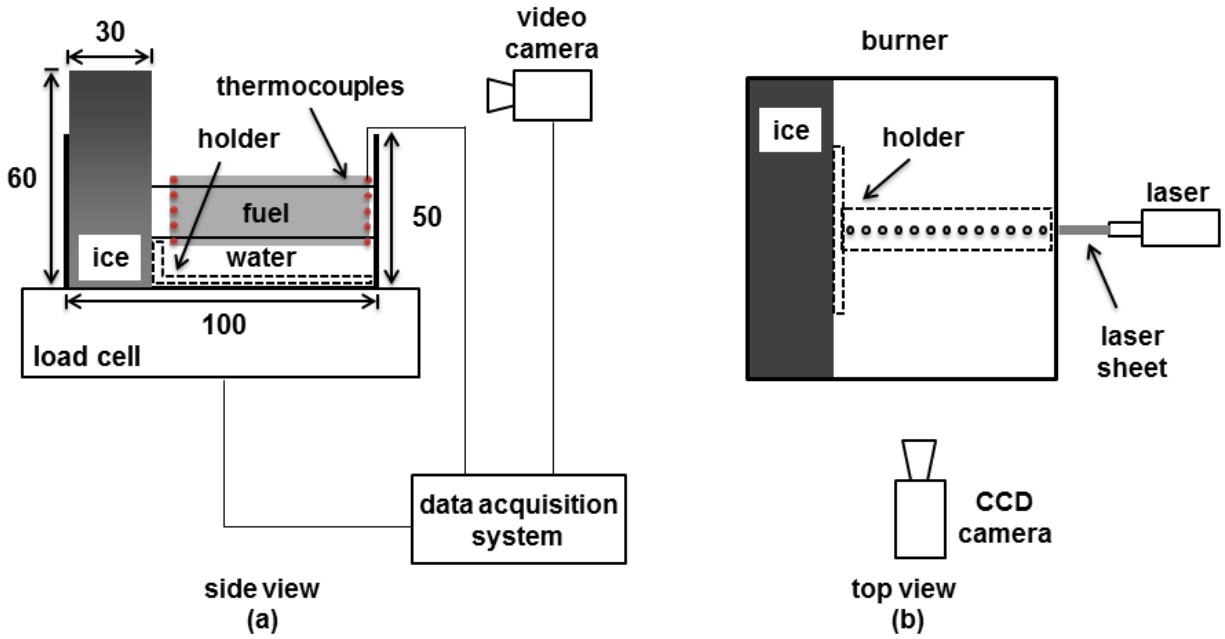

Figure 1. Schematic of the experimental setup. (a) side view of the tray showing the water and fuel layer bound by ice, shaded area corresponds to field of view (b) top view of the tray with PIV setup. The dimensions are in mm.

The velocity field on the mid-plane of the liquid fuel perpendicular to the ice wall was obtained by PIV measurements. The specifications of the PIV equipment used in this study are provided in Table 1. The liquid fuel in the tray was seeded with 10 μm silver coated hollow glass sphere particles. The particles specific gravity, relaxation time, and settling velocity were 1.1, 0.11 μs and 0.27 μm/s, respectively. The shaded area in Fig. 1(a) shows the field of view for the camera. The location of the laser sheet for the velocity measurements is shown in Fig. 1(b). The camera was placed perpendicular to the laser that illuminated a thin light sheet in the flow.

Table 1

Details of the PIV equipment used in the current study

Laser	Type	Nd:YAG, NewWave Solo (Neodym–Yttrium–Aluminum–Granat)
	Energy/pulses	100 mJ/pulse
	Wavelength	532 nm (frequency doubled)
CCD camera	Type	HiSense 12 bit
	Resolution	1280 × 1024 pixel (32 × 32 pixel interrogation area with 50% overlapping)
Particles		Silver coated hollow glass sphere, 10 μm
Software		Flowmanager, Dantec Dynamics

Five thermocouples (K-type, wire and bead diameter of 0.10 mm and 0.25 mm) were also used to measure the temperature of the fuel in the vertical mid-plane perpendicular to the ice. These thermocouples were arranged vertically with 5 mm intervals (see Fig 1(a), with detail shown as solid circles). The ends of the thermocouple wires were parallel to the fuel surface to minimize conduction loss. The radiation loss was assumed to be negligible due to low temperature in the liquid phase. The experimental procedure included moving the thermocouple array for each test in 5 mm increments, creating over the course of the experiments a temperature map of the fuel 20 mm × 60 mm, with a 5 mm resolution (see Fig. 1(a), shaded area representing the temperature map position). The bracket-shape holder that was used to fix the ice at the side of the tray was designed to act as a holder for positioning the thermocouple array at designated locations for each test.

3. Results and Analysis

The geometry change of the ice was monitored with the CCD camera to obtain melting front velocity. In addition, measurements of mass loss over time as well as the video taken from the flame were used to evaluate the burning behavior of the n-octane with and without the ice wall in

the tray. The results are reported in Section 3.1. Results of the PIV study showing the flow field within the fuel layer is presented in Section 3.2. Finally, the results of the temperature analyses are reported in Section 3.3.

3.1. Geometry change due to melting and burning behavior

The experiments started with igniting n-octane over a 20 mm water sub-layer while the ice wall was placed on one side of the tray. As expected based on observations of the previous studies [20, 23], the melting of the ice was more significant in the regions of the fuel layer contact with the ice wall versus regions of flame impingement. Thus, the fuel layer created a void in the ice which eventually led to the splitting and falling of the top section into the pool. Figure 2 shows the splitting sequence from the beginning to the end of an experiment. The ice, n-octane and water are labeled in Fig. 2a.

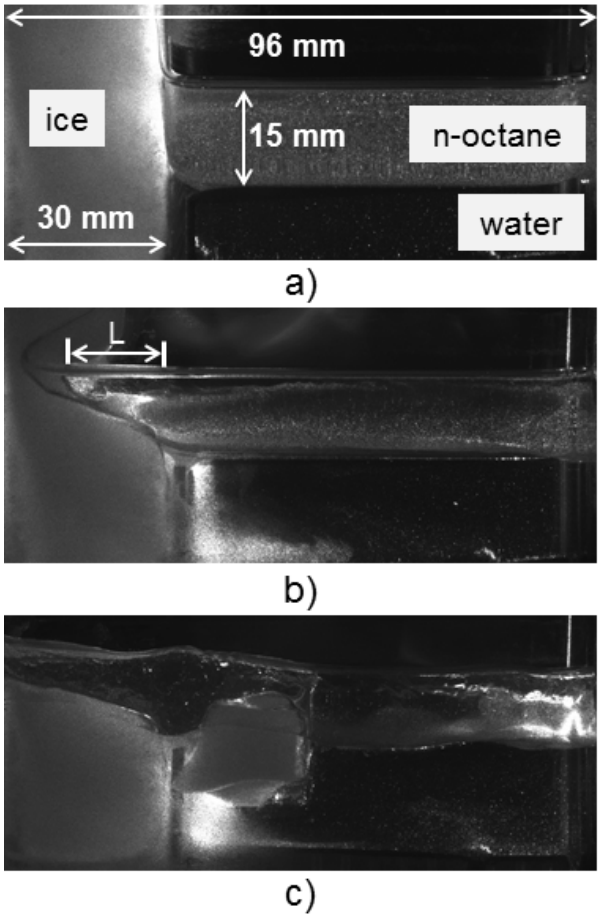

Figure 2. Melting process of the ice in the tray with ice on the left and n-octane on top of water layer on right. a) before ignition, b) 130 seconds after ignition, and c) splitting after 195±5 seconds. The ice was made with tap water for better illustration in this figure.

Figure 3 shows the intrusion of the fuel layer into the ice (indicated as penetration length *"L"* in Fig. 2 b) with respect to time. The slope of the lines indicate the melting front velocity. Three distinct periods with different values of melting front velocity are identified in Fig. 3. In the period before ignition, minor melting occurs due to higher ambient and pool temperatures with the melting front velocity of around 0.04 cm/min. This has an important implication for lateral cavity formation in arctic oil spill, as the sunlight can potentially contribute in ice melting due to the high emission absorptivity of crude oils. After igniting the fuel and in the first 50 seconds (Phase 1), the melting front velocity was measured to be around 0.6 cm/min. In the rest of the burning time (Phase 2), the melting front velocity was measured 1 cm/min.

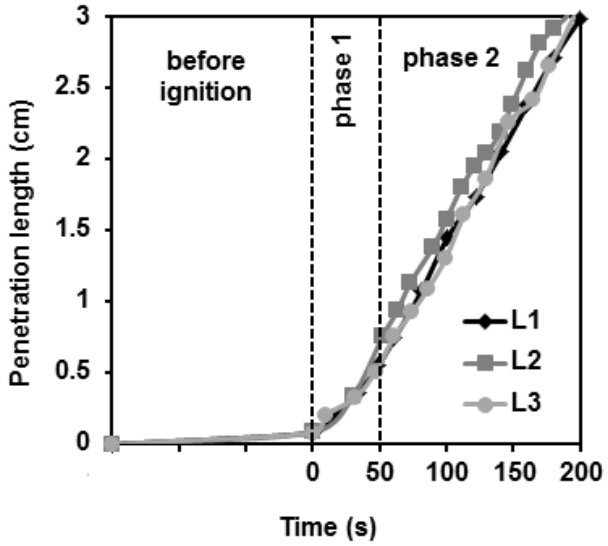

Figure 3. Penetration length of the fuel in the ice over the burning time for three experiments labeled as *L_1, L_2, and L_3*. The melting front velocity (slope of the curve) is roughly 0.04 cm/min for the period before ignition, 0.6 cm/min in the first phase, and 1 cm/min in the second phase.

The mass loss rate and flame height from 3 identical experiments are compared and their average trend is reported. Experiments with similar initial conditions but without the ice wall in the tray were also performed to compare the burning behavior of the fuel with and without the ice in the tray. The thickness of the fuel layer was initially at 15 mm (equal to 73 g of n-octane) and reduced to 11.5 mm (60 g) at the end of the experiment. However, because of the accumulation of melt-water under the fuel layer, the fuel layer was slightly elevated with respect to the bottom of the tray at the end (~3 mm). The measurements were stopped after the ice top detached for the tests with ice wall. The splitting of the ice was used as an end-point to the experiments, and

occurred consistently after 195±5 seconds. During the ~200 second burn, 13.1 g of n-octane was consumed in each test with ice present, giving an average burning rate of 0.066 g/s, while tests performed without the ice wall consumed 16.4 g of n-octane giving an average burning rate of 0.082 g/s. The average burning rate per unit area of the tray was 8.6 g/s.m^2 for ice wall tests, compared to 8.9 g/s.m^2 for tests without an ice wall. Because the ice occupied a portion of the tray and gradually melted away, the average burning rate per unit area of the experiments with ice was calculated based on an average area (96×80 mm). The reduction in the overall surface area of the pool in the presence of ice was the main reason for the lower burning rates in the cases with ice. Figure 4, shows the averaged mass loss rate during the 200 seconds burning of n-octane. The experiments with the ice wall present in the tray are shown with dotted line, and the experiments without the ice wall are presented with dashed line.

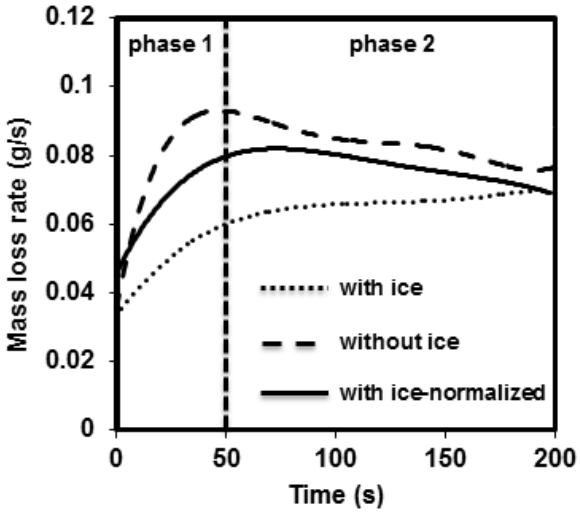

Figure 4. Mass loss rate of n-octane over the time for experiments with and without the ice wall. The case with ice is normalized to account for the reduced burning area of the fuel due to the presence of the ice.

Phases 1 and 2, as shown in Fig. 3, are also identified in the mass loss rate trends in Fig. 4. In the tests without the ice wall, the mass loss rate increased with time and reached a maximum value at around 50 seconds. During this period the ullage distance also increased due to surface regression. As a result, after a point, the mass loss rate gradually decreased, because an increase in the ullage decreases the transport of oxygen and heat towards the surface. On the other hand, the mass loss rate showed only an increasing trend for the case with ice. This is due to the fact that as the ice melts the water level beneath the pool surface increases and this reduces the ullage

distance. As mentioned, one of the reasons for the lower burning rate for the case with ice is the reduction in the pool surface area. A third curve is added to Fig. 4 (solid line) representing the normalized mass loss rate of n-octane with ice. This curve is normalized based on the available surface area of the fuel to burn (the surface area of the tray minus the area occupied by the ice wall). The normalized curve provides a comparison of the mass loss rate of the two cases without the influence of geometry (equal surface area for the fuel to burn). As can be seen, the presence of ice (with the assumption of similar surface area) has minimal effect on the burning rate. The lower burning rate in the normalized case may be attributed to the fact that n-octane has heat losses to the ice. Thus, for the same heat flux received from the flame, the case with ice burns at a slower rate than the case without ice.

Figure 5 shows the results of flame height analysis for the case with and without the ice wall. The tests with ice show slightly smaller flame height compared to the case without the ice. The flame heights results for both experiments showed a period of growth within the first 50 seconds of experiments (Phase 1) before reaching a steady fluctuating phase (Phase 2). The vertical line in Fig. 5 separates the two phases.

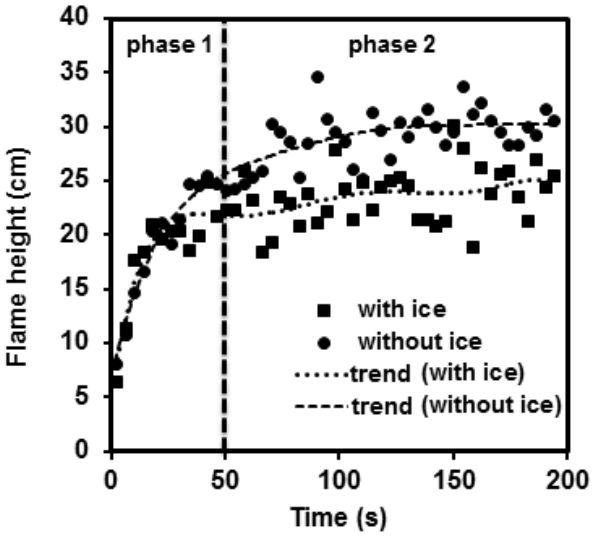

Figure 5. Flame height of n-octane over the time for experiments with and without the ice wall.

3.2. Velocity Field

The flame impingement on the fuel surface and the presence of the ice alongside the n-octane pool created a convective field for the transfer of heat and mass in the fuel layer. The heat received on the fuel surface increased the free surface temperature to sustain the burning and the rest was transferred towards heating the liquid portion below the surface and the ice wall. In an earlier study [23], it was hypothesized that the melting of the ice wall is related to the convective motions in the liquid phase. In this study the hypothesis was examined through flow visualization and careful analysis of the flow structure. The buoyant and surface tension forces can be considered as the driving forces for convection within the liquid-phase of the pool fire that contributed to the melting of ice and formation of the lateral cavity [26, 27]. The Grashof and Marangoni numbers corresponding to the convective flow in the fuel layer [28, 29] can be expressed as

$$Gr = \frac{\partial \rho}{\partial T} \frac{g \Delta T_v H^3}{\vartheta \mu}, \qquad (1)$$

$$Ma = \left|\frac{\partial \sigma}{\partial T}\right| \frac{\Delta T_h R}{\mu \alpha}, \qquad (2)$$

where R is the half-length of the pool, H is the thickness of the fuel, g is the acceleration due to gravity, and σ, ρ, μ, ϑ, and α are surface tension, density, dynamic viscosity, kinematic viscosity and thermal diffusivity of the liquid, respectively. The vertical temperature difference on the bulk of the liquid can be assumed to be ΔT_v and on the horizontal free surface of the liquid as ΔT_h. Table 2 provides the properties of the fuel and the related experimental measurements that are used to estimate the Grashof and Marangoni number.

Table 2

Properties and dimensions used to calculate Gr and Ma.

n-octane properties at 20 °C (obtained from Aspen HYSYS®)		Regime		Vertical temp. gradient ΔT_v (°C)*	Horizontal temp. gradient ΔT_h (°C)	Liquid fuel height H^3 (m^3)	Half length of the tray R (m)	Grashof and Marangoni number
$\frac{\partial \rho}{\partial T}$ (kg/m^3.K)	0.82	Combined (before ignition)		4.5	5.2	3×10^{-6}	0.03	$Gr_0 \sim 2.6\times10^5$ $Ma_0 \sim 3.2\times10^5$
$\frac{\partial \sigma}{\partial T}$ (N/m.K)	-9.5×10^{-5}							
μ (kg/m.s)	5.46×10^{-4}	Separated (after ignition)	Phase 1	45.8	65.6	2×10^{-6}	0.04	$Gr_1 \sim 1.7\times10^6$ $Ma_1 \sim 5.3\times10^6$
α (m^2/s)	8.6×10^{-8}							
ϑ (m^2/s)	7.76×10^{-7}		Phase 2	109.1	122.2	1×10^{-6}	0.05	$Gr_2 \sim 2.1\times10^6$ $Ma_2 \sim 1.2\times10^7$
g (m/s^2)	9.81							

* The temperature differences are obtained from the experiments.

After the fuel was poured into the glass tray, when both ΔT_v and ΔT_h were low and the magnitudes of Grashof and Marangoni numbers were comparable ($Gr_0 \sim 2.6 \times 10^5$ and $Ma_0 \sim 3.2 \times 10^5$), the flow field showed one combined convection roll with two distinctive group of vectors [28]. The first group induced by the Marangoni effect, created a horizontal flow 3-4 mm below the free surface with a weak return flow for -15 < Y < -4 mm. Figure 6 shows the horizontal velocity profile of the fuel, obtained from PIV measurements 3 and 8 mm away from the ice wall. The Marangoni induced flow had a velocity of 3-4 mm/s below the surface as shown in Fig. 6. The second group of vectors was traveling downward, adjacent to the ice due to the buoyancy effect. The combination of these two flows is representing a combined convection regime due to the coupling of thermocapillary and buoyancy forces.

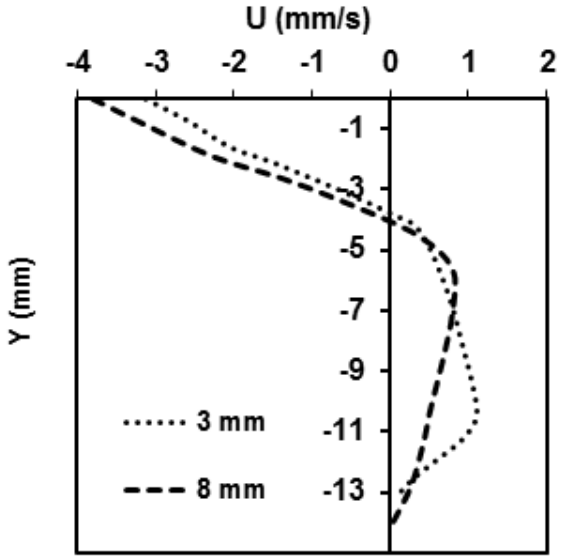

Figure 6. Horizontal component of velocity (U) over the fuel depth at 3 mm and 8 mm away from the ice wall obtained from PIV measurements.

The velocity field of the liquid fuel on the vertical mid-plane prependicular to the ice wall was measured by the PIV system described in section 2. The coupling of thermocapillary and buoyancy in the combined regime (before ignition), and formation of a large convection roll in the flow field near the ice wall is shown in Fig. 7. Figure 7 (a) and (b) show the velocity vector field overlaid on the velocity magnitude map and streamlines of flow with background map of vorticity magnitude, respectively. The return flow is apparent on the lower left side of the domain in Fig 7a. The maximum velocity magnitude of 4-5 mm/s was found below the free surface and near the ice. The streamlines of flow showed a large convective roll covering the whole domain with vorticity magnitude of less than 2 s^{-1}. The pattern of the flow and the convective roll formed in the liquid fuel before ignition corroborates the hypothesis that was proposed in the previous study by the authors [23]. However, the flow measurement after ignition revealed a more complicated flow field than what was anticipated.

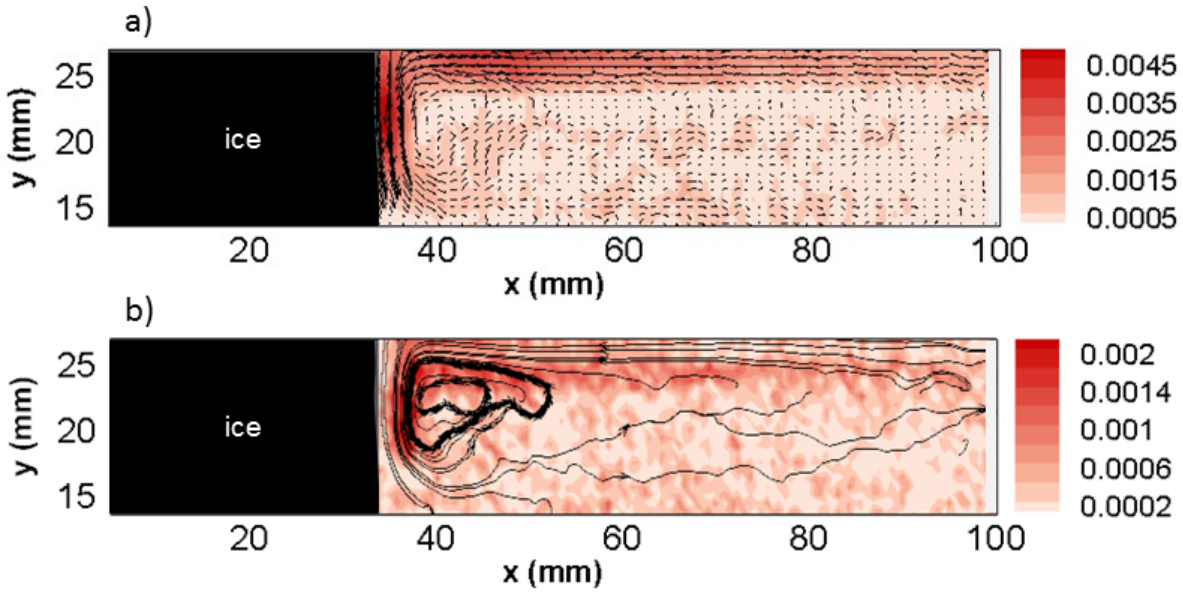

Figure 7. Flow field of n-octane before ignition a) The vector field with background color map of velocity magnitude (m/s) b) Streamlines of flow with background color map of vorticity magnitude ($s^{-1} \times 10^{-3}$).

After ignition, impingements of the growing flame on the fuel surface increased the temperature differences (ΔT_v and ΔT_h), and thereby augmenting the Grashof and Marangoni numbers ($Gr_1 \sim 1.7 \times 10^6$ and $Ma_1 \sim 5.3 \times 10^6$). An unstable flow regime denoted as separated regime (Table 2) started due to the increase and dominance of the Marangoni over Grashof number. Phase 1 (the first ~40 seconds after ignition) began with individual vortices traveling toward the ice and ended with presence of the multi-roll structure near the fuel surface. During the first phase, a multi-roll structure began to appear due to separation of buoyant and surface tension forces [30]. The flow field 10 seconds after ignition, as seen in Fig. 8, shows a main counter clockwise vortex. Figures 8 (a) and (b) show the velocity vector field overlaid on the velocity magnitude map and streamlines of flow with background map of vorticity magnitude, respectively. As expected, after ignition the velocity magnitudes increased and more regions of the fuel became involved in convective flows. The maximum velocity of 8 mm/s was measured to occur below the fuel surface. As shown in Fig. 8 (b) the counter clockwise rotating vortex was formed in the upper half and near the fuel surface that moved toward the ice with a vorticity magnitude of 4 s^{-1}. The vorticity color map also shows that most of the rotations occur near the fuel surface.

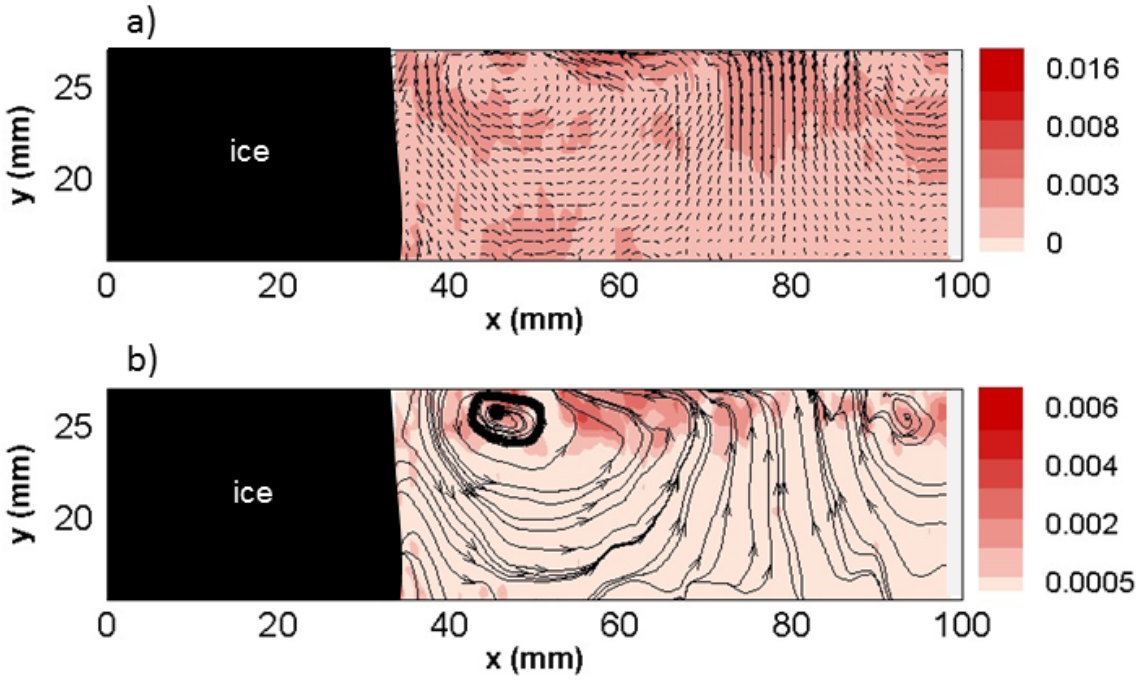

Figure 8. Flow field of n-octane 20 seconds after ignition a) The vector field with background color map of velocity magnitude (m/s) b) Streamlines of flow with background color map of vorticity magnitude ($s^{-1} \times 10^{-3}$).

As the flame heights/burning rate increased, complete separation of buoyant and surface tension flows initiated the multi-roll structure layer with axes of the rolls parallel to the ice wall (below the free surface of the fuel and near the ice) [29, 31]. The multi-roll layer separated from the main flow, with thickness of 3-4 mm, and consisted of many rotating waves with relatively small radii that were visually observable through the tray walls. In pool fire literature, the multi-roll layer structure is introduced by the name of *inversion layer* and is stated to be driven by the thermal instabilities caused by buoyancy only [15, 32, 33]. However, near the ice wall, horizontal temperature difference, and consequently surface tension driven instabilities also seems to play an important role in the formation of the inversion layer.

Figure 9 (a) and (b) show velocity vector field overlaid on the velocity magnitude map and streamlines of flow with background map of vorticity magnitude, respectively. The flow field became more complex and showed a significant change in the magnitudes and pattern as the pool surface was extended into the ice cavity. Still, the downward movement of the liquid near the ice surface remained intact. The maximum velocity magnitude was expected to be seen below the surface and near the ice, but the multi-roll structure repelled the seeding particles and made the

measurments to be partially insufficient. Thus, the maximum velocity magnitude was recorded around 16 mm/s in the middle of the pool.

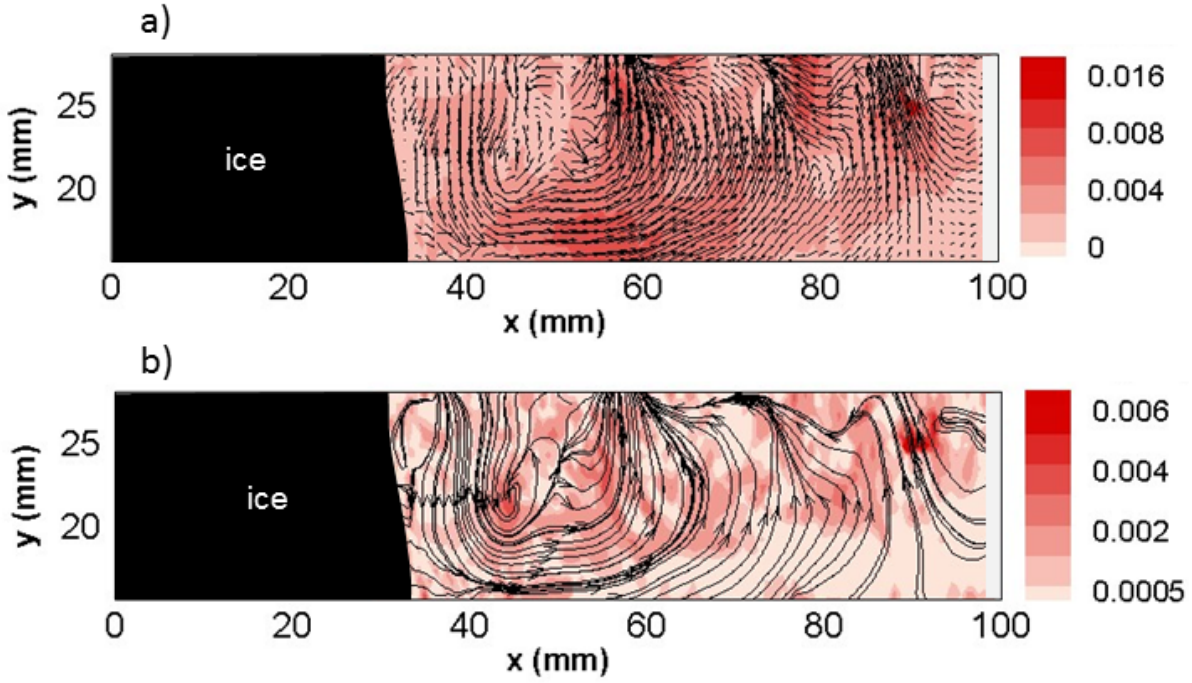

Figure 9. Flow field of n-octane 40 seconds after ignition a) The vector field with background color map of velocity magnitude (m/s) b) Streamlines of flow with background color map of vorticity magnitude ($s^{-1} \times 10^{-3}$).

The separation of buoyant and surface tension forces in Phase 1 resulted in the appearance of the single traveling vortex initially and then to the creation of the multi-roll structure. The multi-roll structure remained intact for the rest of the burning period. When the flame heights/burning rate reached their maximum in the second phase, both ΔT_v and ΔT_h increased significantly, resulting in $Gr_2 \sim 2.1 \times 10^6$ and $Ma_2 \sim 1.2 \times 10^7$. The term spatiotemporal chaos is used herein to describe a constantly varying instantaneous velocity field with high velocity magnitudes mainly because of an increase in the Marangoni number to around 1.2×10^7 in the second phase.

The PIV measurements were rather difficult in the liquid after the onset of the 3-dimensional unsteady flow during the second phase of the burning. Presence of the ice in the liquid pool intensified the temperature differences and consequently complicated the system further. The quality of images that were taken after ignition slowly started to deteriorate. Two major issues made the PIV measurements less useful after about 40 seconds. Figure 10 (a) shows these issues from an image that was taken after 50 seconds from the ignition. Labeled areas in Fig. 10 (a)

show the dark, blurry, and stretched region numbered 1 and 2, respectively. The first issue (label 1) was a dark region without tracer particles which corresponds to the location of the multi-roll structure. This dark region started to appear near the ice during Phase 1 and was stretched to the entire pool length by the end of experiments. The centrifugal force acting on the particles in the multi-roll layer repelled the particles thus a black region was seen in the images [34]. As shown in Fig. 10 the thickness of this region was greater near the ice which shows the higher intensity of the rolls near the ice wall. Region 2 depicts the formation of a blurry area in the vicinity of the ice wall, which may be caused by mixing of hot fuel heated by the flame and cold fuel cooled by the ice. Region 3 originates because of the high temperature variation and subsequent variation in the refractive index of the fuel. The scattered light from tracer particles was stretched and distorted arbitrarily causing high measurement uncertainty. The vector field shown in Fig. 10 (b) is produced by an image pair of which one is depicted in Fig. 10 (a). While the vector field near the ice is not representing the actual displacement of the liquid due to the absence of tracer particles, an instantaneous downward flow in the middle of the pool and below the surface with high velocity magnitudes is observed. A maximum velocity of around 20 mm/s was observed for this region, but greater velocities are expected to have occurred closer to the ice.

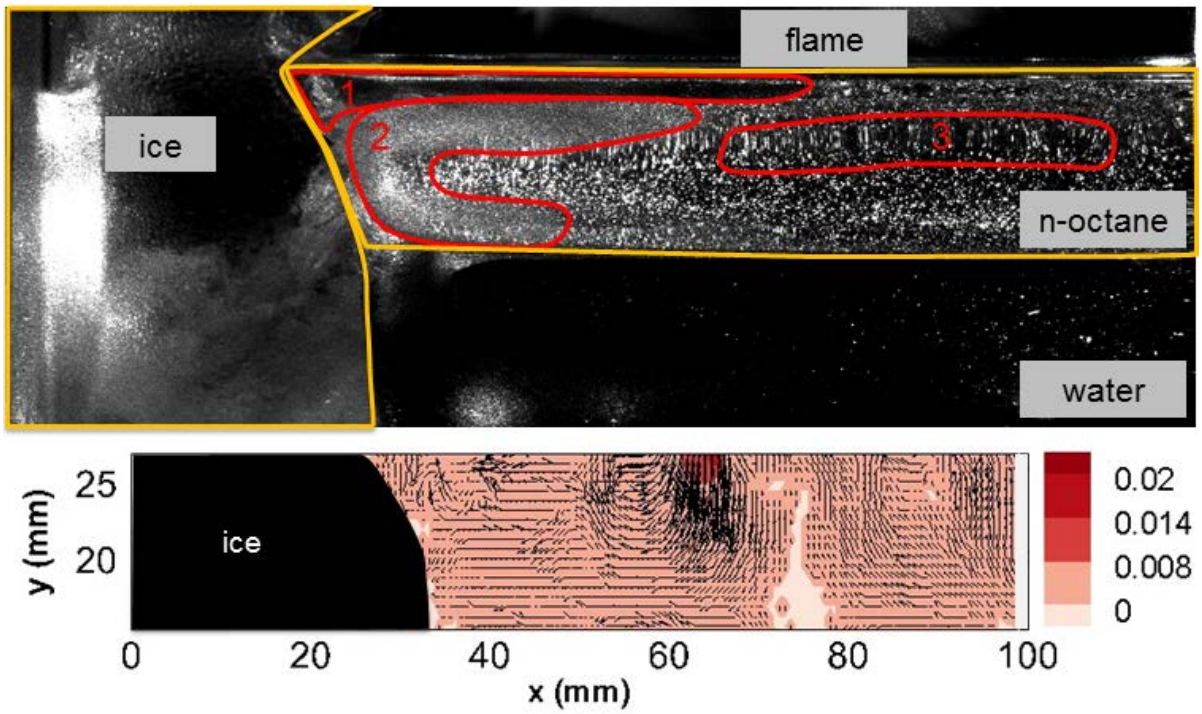

Figure 10. Deterioration of PIV image qualities after 50 seconds from ignition on top. The different types of issues are labled by numbers in the top image (9.5 cm length by 4 cm

height). The vector field of n-octane layer obtained from the same image with background color map of velocity magnitude (m/s) on the bottom.

An earlier study by the current authors [24] introduced two major convective flows (natural and Marangoni convection) as the driving force for convection in a burning fuel layer adjacent to ice. The two convection mechanisms were also used to demarcate different melting rates that occur in a lab-scale pool fires in an ice cavity. Herein, the convective flows were examined by observations with a PIV system and also through Gr and Ma numbers. Also, the convective regimes (characterized by magnitude of Gr and Ma numbers) that relate to two distinct melting rates were evaluated herein. The extensions of these results to a larger scale or fuels that are multi-component require additional information and validation experiments at larger scales (1 to 30 m), as discussed by Emori and Saito [24], and is thus beyond the scope of the current study.

3.3. Temperature Field

As part of this study, the temperature field of the fuel layer was measured by a thermocouple array as described in Section 2. Contours of temperature within the liquid phase are shown in Fig. 11 (a-e) (with the ice on the left side). The temperature contours are plotted with linear interpolation in x and y direction. The thermocouple positioned at the top of the array recorded the temperature of the gas phase and because melting of the ice caused the fuel layer to rise, it eventually recorded the temperature of n-octane surface. The elevation of the top surface and interface of the fuel-water were tracked via the images obtained from the PIV experiments and are presented in Fig. 11 to detail the fuel layer displacement. Note that the top layer elevates during time. The red solid line in Fig. 11 shows the interface of the fuel-water. The thermocouple at the bottom of the array remained in the water layer and recorded the temperature of the water layer only. The boiling point temperature of n-octane (125 ℃) was assigned to the top layer.

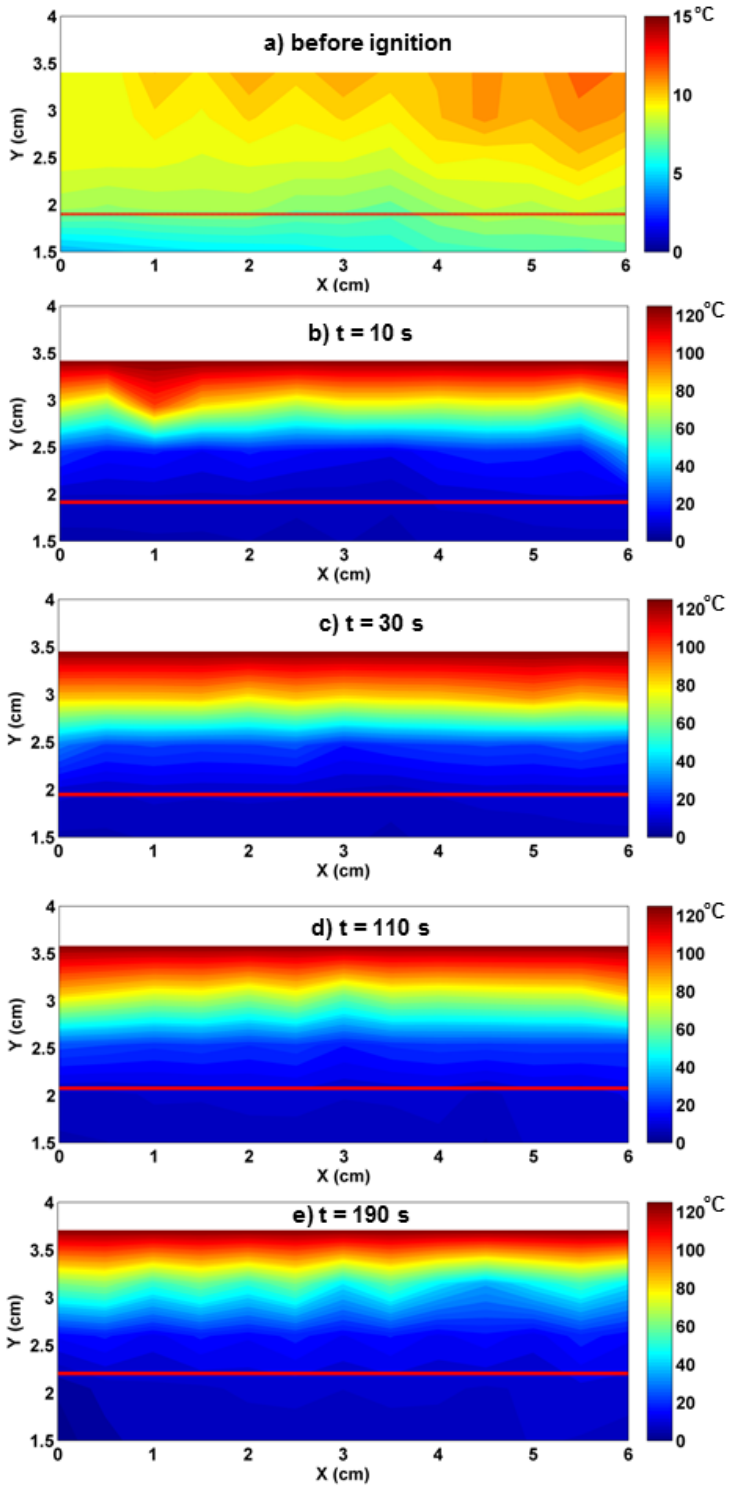

Figure 11. Temperature (℃) distribution within the liquid phase of n-octane pool fire with ice wall located on the left side of the fuel (t = 0 s is the moment of ignition). a) before ignition, b) t = 10 s, c) t = 30 s, d) t = 130 s, e) t = 190 s. The red line shows the fuel-water interface.

Figure 11(a) shows the temperature distributions before ignition along the vertical direction of the fuel layer. Due to the proximity of the ice wall on the left side of the contours, lower temperatures were recorded in this area. After ignition (Fig. 11 (b-e)), the temperature distributions showed a two-layer thermal structure within the liquid fuel. The upper layer with a temperature range of 60 – 125 ℃ had a steep temperature gradient in the vertical direction. This layer maintained a thickness of approximately 8 mm as the fuel burned. The top section of the upper layer (hot zone), with temperature range of above 100 ℃ and thickness of about 3 mm, corresponding to the location of the multi-roll layer greatly contributed in the ice melting process. In contrast, the lower layer remained relatively cold for the entire length of the experiments. Also, a gradual decrease of temperature in horizontal direction and toward the ice, top left side of the Fig 5 (b), was observed which is due to the presence of the ice in the early stage of burning.

Figure 12 shows the ice shape and the fuel layer location around 160 seconds after ignition of the fuel. The unstable flow regime and the multi-roll structure in the upper layer of the fuel is clearly visible in Fig. 12. The structure was experimentally observed to originate near the ice wall and expand horizontally with the progress in burning. The wavy line in Fig. 12 shows the lower boundary of the multi-roll layer that was stablished during Phase 2. This implies the presence of a strong transport mechanism in the upper fuel layer that is responsible for the transfer of heat (flame feedback) towards the ice wall. In addition, the fuel layer had horizontal parallel isotherms at the beginning of the burning period ($t = 10$ and 30 s) indicating a uniform temperature distribution in Phase 1. Later in the experiments (Phase 2), the isotherms became wavy, which is most obvious in Fig. 11 (e). The waviness of the isotherms may be attributed to the presence of the multi-roll and the chaotic state of the flow in the latter stage of the burning.

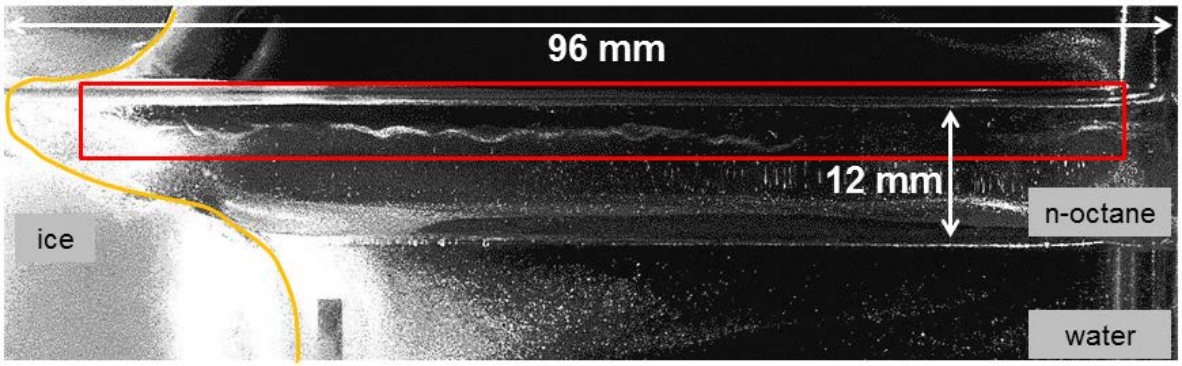

Figure 12. The ice wall (yellow line) and location of the fuel layer shown by an image taken about 160 seconds after ignition. The wavy line below the free surface (enclosed by the red rectangle) shows the lower boundary of the multi-roll structure.

Conclusions

A previous study showed that the melting of ice near a pool fire was related to the convective motions within the liquid-phase of the pool fires. In order to examine this hypothesis, a series of experiments were conducted to understand the thermal and flow field of n-octane burning adjacent to an ice wall.

Experiment showed that the melting front velocity increase after ignition in two different steps (phases 1 and 2). Before ignition, a combined flow in the fuel layer was established toward the ice (with maximum velocity of 4 mm/s) due to coupling of Marangoni convection and buoyancy. However, after ignition both magnitude and shape of the flow field changed significantly. Transition from combined one roll structure to multi-roll structure followed by spatiotemporal chaos occurred due to the increase in the temperature differences caused by flame impingement. The velocity magnitude increased and reached 16 mm/s in the transition period. At the same time, the vorticity magnitude increased and most of the fuel layer became involved with convective currents. The increased velocity in the separated regime (multi-roll structure) could be the main cause of the melting of the ice. Based on the thermocouple measurements, a two layer thermal structure; 1) a top layer with steep temperature gradient in the vertical direction and 2) a low temperature zone was observed in the fuel layer. The ice melting was much more significant in the upper layer regions of contact where the multi-roll structure was present.

An in-depth analysis of the flow characteristics requires an understanding of the influence of thermo-physical properties of the liquid during the complex process of convection-driven melting. Therefore, a parametric study on the convection-melt phenomenon using liquids with different thermal properties and controlled temperatures could potentially clarify the dominant parameters on melting.

Conflicts of interest

The contents do not necessarily reflect the views and policies of the BSEE, nor does mention of the trade names or commercial products constitute endorsement or recommendation for use.

Acknowledgement

We thank Jianhua Fan and Simon Furbo for letting use their PIV system, and Knud Erik Meyer,

Hayri Sezer, and Shijin P.Kozhumal, for their comments that greatly improved the manuscript. This study was partially funded by the Bureau of Safety and Environmental Enforcement (BSEE), US Department of the Interior, Washington, DC, under Contract Number E14PC00010. Hamed Farmahini Farahani and Grunde Jomaas were supported by the Danish Council for Independent research (Grant DDF – 1335-00282).

References

[1] H. D. Ross, Ignition of and Flame Spread Over Laboratory-Scale Pools of Pure Liquid Fuels, *Prog. Energy Combust. Sci.* 20 (1994) 17-63.
[2] F. J. Miller, H. D. Ross, Further observations of flame spread over laboratory-scale alcohol pools, *Symposium (International) on Combustion*, (1992), 1703-1711.
[3] J. Burgoyne, A. Roberts, P. Quinton, The spread of flame across a liquid surface. I. The induction period, *Proceedings of the Royal Society of London. Series A. Mathematical and Physical Sciences* 308 (1968) 39-53.
[4] I. Glassman, J.G. Hansel, *Fire Research Abstracts and Reviews* 10 (1968) 217-234.
[5] R. Murad, J. Lamendola, H. Isoda, M. Summerfield, A Study of Some Factors Influencing the Ignition of a Liquid Fuel Pool *Combustion and Flame* 1 (1970) 289-298.
[6] R. J. Murad, "Experimental Investigation of Ignition of Pools of Liquid Hydrocarbon Fuels," M.S. Thesis, , Princeton university, 1970.
[7] R. McKinven, J. G. Hensel, I. Glassman, Influence of laboratory parameters on flame spread over liquid surfaces, *Combustion Science and Technology* 1 (1970) 293-306.
[8] A. Ito, D. Masuda , K. Saito, A Study of Flame Spread Over Alcohols Using Holographic Interferometry, *Combustion and Flame* 83 (1991) 375-389.
[9] K. E. Torrance, Subsurface flows preceding flame spread over a liquid fuel, *Combustion Science and Technology* 3 (1971) 133-143.
[10] K. E. Torrance, R. L. Torrance, Fire spread over liquid fuels: Liquid phase parameters, *Symposium (International) on Combustion* 15 (1975) 281-287.
[11] K. Takahashi, A. Ito, Y. Kudo, T. Konishi, K. Saito, Scaling analysis on pulsating flame spread over liquids, *International Journal of Chemical Engineering* (2008.)
[12] I. Glassman, F. Dryer, Flame Spreading Across Liquid Fuels, *Fire Safety Journal* 3 (1980/81) 123 - 138.
[13] T. Yumoto, A. Takahashi, T. Handa, Combustion Behavior of Liquid Fuel in a Small Vessel: Effect of Convective Motion in the Liquid on Burning Rate of Hexane in the Early Stage of Combustion, *Combustion and Flame* 30 (1997) 33-43.
[14] A. Vali, D. S. Nobes, L. W. Kostiuk, Transport phenomena within the liquid phase of a laboratory-scale circular methanol pool fire, *Combustion and Flame* 161 (2014) 1076-1084.
[15] A. Ito, K. Saito, T. Inamura, Holographic interferometry temperature measurements in liquids for pool fires supported on water, *Journal of heat transfer* 114 (1992) 944-949
[16] S. L. Ross, "Tests to Determine the Limits to In Situ Burning of Thin Oil Slicks in Broken Ice," Report to Minerals Management Service and ExxonMobil Upstream Research. Herndon, VA, U.S.2003.
[17] D.F. Dickins, I. Buist, "Oil and Gas Under Sea Ice," Prepared by Dome Petroleum Ltd CV-1, 1981.

[18] I. Buist, D. Dickins, Experimental spills of crude oil in pack ice, *International Oil Spill Conference*, (1987), 373-381.
[19] A. Nakakuki, Heat Transfer Mechanisms in Liquid Pool Fires, *Fire Safety Journal* 13 (1994) 339-363.
[20] H. F. Farahani, X. Shi, A. Simeoni, A. S. Rangwala, A study on burning of crude oil in ice cavities, *Proc. Combust. Inst.* 35 (2014) 2699-2706.
[21] P. W. Bellino, A.S. Rangwala, M.R. Flynn, A study of in situ burning of crude oil in an ice channel, *Proc. Combust. Inst.* 34 (2013) 2539-2546.
[22] X. Shi, P. Bellino, A. Simeoni, A. Rangwala, Experimental study of burning behavior of large-scale crude oil fires in ice cavities, *Fire Safety Journal* 79 (2016) 91-99.
[23] H. F. Farahani, G. Jomaas, A. S. Rangwala, Effects of convective motion in n-octane pool fires in an ice cavity, *Combustion and Flame* 162 (2015) 4643-4648.
[24] R. I. Emori, K. Saito, A study of scaling laws in pool and crib fires, *Combustion science and technology* 31 (1983) 217-231
[25] C. A. Schneider, W. S. Rasband, K. W. Eliceiri, NIH Image to ImageJ: 25 years of image analysis, *Nat methods* 9 (2012) 671-675.
[26] D.N Schiller, W.A Sirignano, Buoyant-Thermocapillary Flow with Nommiform Supra-Heating: I. Liquid-Phase Behavior, *J. Thermophysics* 6 (1992) 105-112.
[27] D.N Schiller, W.A Sirignano, Buoyant- Thermocapillary flow with nonuniform supra heating: II. Two phase behavior, *J. Thermophysics* 6 (1992) 113-120.
[28] T. Song, Comparison of buoyancy and surface tension in a square cavity, *KSME Journal* 5 (1991) 10-15.
[29] D. Schwabe, J. Metzger, Coupling and separation of buoyant and thermocapillary convection, *Journal of Crystal Growth* 97 (1989) 23-33.
[30] D. Villers, J. Platten, Coupled buoyancy and Marangoni convection in acetone: experiments and comparison with numerical simulations, *Journal of Fluid Mechanics* 234 (1992) 487-510
[31] D. Schwabe, A. Cramer, J. Schneider, S. Benz, J. Metzger, Experiments on the multi-roll-structure of thermocapillary flow in side-heated thin liquid layers, *Advances in Space Research* 24 (1999) 1367-1373.
[32] M. Arai, K. Saito, R. Altenkirch, A Study of Boilover in Liquid Pool Fires Supported on Water Part I: Effects of a Water Sublayer on Pool Fires, *Combustion Science and Technology* 71 (1990) 25-40.
[33] T. Inamura, K. Saito, K. Tagavi, A study of boilover in liquid pool fires supported on water. Part II: Effects of in-depth radiation absorption, *Combustion science and technology* 86 (1992) 105-119.
[34] G. Falkovich, A. Pumir, Intermittent distribution of heavy particles in a turbulent flow, *Physics of Fluids* 16 (2004) L47-L50.